Applied Energy 360 (2024) 122825

Contents lists available at ScienceDirect

Applied Energy

journal homepage: www.elsevier.com/locate/apenergy

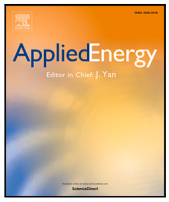

A transferable long-term lithium-ion battery aging trajectory prediction model considering internal resistance and capacity regeneration phenomenon

Yaodi Huang [a,1], Pengcheng Zhang [b,1], Jiahuan Lu [c], Rui Xiong [c,*], Zhongmin Cai [a,*]

[a] MOE KLINNS Lab, School of Automation Science and Engineering, Xi'an Jiaotong University, Xi'an, 710054, People's Republic of China
[b] Center for Advancing Materials Performance from the Nanoscale (CAMP-Nano), State Key Laboratory for Mechanical Behavior of Materials, Xi'an Jiaotong University, Xi'an, 710049, People's Republic of China
[c] National Engineering Laboratory for Electric Vehicles, School of Mechanical Engineering, Beijing Institute of Technology, Beijing, 100081, People's Republic of China

ARTICLE INFO

Dataset link: https://data.mendeley.com/datasets/56hdnvr7hs

Keywords:
Capacity regeneration phenomenon
Lithium-ion batteries
Neural network
Remaining useful life
Transfer learning

ABSTRACT

Accurately predicting the remaining useful life (RUL) of lithium-ion batteries (LiBs) is crucial for improving battery management system design and ensuring device safety. However, achieving accurate long-term predictions of aging trajectories is challenging due to error accumulation in multi-step ahead forecasts. This study shows that considering future internal resistance (*R*), which is related to the aging process, and the capacity regeneration phenomenon (CRP) that occurs during aging can help reduce error accumulation. Specifically, we propose a hybrid method that incorporates future *R* and CRP to predict the aging trajectories and RULs of LiBs. Experiment results demonstrate: (1) for the same charging/discharging policies and battery types, the proposed method can accurately predict the aging trajectory and RUL using only the first 20 cycles' data (approximately 5% of the complete data); (2) for different charging/discharging policies and battery types, with transfer learning, the proposed method can predict the aging trajectory and RUL using the first 40 cycles' data. These results demonstrate that the proposed model is both accurate in long-term prediction and robust for estimating the aging trajectory and RUL across various datasets.

1. Introduction

Lithium-ion batteries (LiBs) are extensively utilized in various fields, such as electric vehicles (EVs), consumer electronics, and aerospace systems, due to their high energy density, low self-discharge rates, and extended lifetimes [1–3]. However, the usage and storage of LiBs lead to degradation, resulting in escalated maintenance costs, downtime, and potential hazardous incidents. To ensure the efficiency and safety of LiBs, the battery management system (BMS) holds practical significance. The BMS is a vital component that plays a crucial role in the monitoring, control, and protection of LiBs throughout their life cycle. As core functions of BMS, accurate state of health (SOH) estimation and remaining useful life (RUL) prediction of LiBs are essential for optimizing energy management and improving battery safety [4].

SOH refers to the extent of battery aging and is often quantified by the capacity fade and increase in internal resistance (*R*) [5]. RUL represents the number of cycles that a battery can undergo before reaching its end-of-life (EOL) threshold, which is typically defined when battery capacity declines to 80% of its initial value [6]. As users pay more attention to the future lifespan of LiBs, the accurate prediction of the aging trajectory and RUL becomes of paramount concern.

1.1. Literature review and motivations

Aging trajectory prediction methods are utilized to estimate the RULs of batteries by extrapolating their capacity or SOH degradation trajectories. In general, aging trajectory prediction methods include model-based methods, data-driven methods, and hybrid methods. Model-based methods involve developing a physical model for aging trajectory prediction based on various aging mechanisms of a battery, such as the formation of solid electrolyte interphase (SEI) layer, loss of the active materials, lithium plating, etc. [7]. Although aging trajectory and RUL can be obtained through model-based methods, there are too many parameters that require identification, and the partial

* Corresponding authors.
E-mail addresses: zmcai@mail.xjtu.edu.cn (Z. Cai), rxiong@bit.edu.cn (R. Xiong).
[1] These two authors contribute equally to this study.

https://doi.org/10.1016/j.apenergy.2024.122825
Received 3 May 2023; Received in revised form 27 November 2023; Accepted 6 February 2024
Available online 17 February 2024

differential and algebraic equations also results in a heavy computational burden [8].

Instead of modeling a physical model to simulate the complex and nonlinear battery aging mechanisms, data-driven techniques such as machine learning (ML) and deep learning (DL) offer an alternative approach. These techniques learn battery aging behavior from historical aging trajectories or health-related features to construct future aging trajectories. By analyzing the historical aging trajectories, Zhang et al. [9] proposed a long short-term memory (LSTM) network to learn the long-term dependencies among the capacities of LiBs. This LSTM model was then employed for predicting future aging trajectories. Similarly, Guo et al. [10] developed a relevance vector machine (RVM)-based model and Ma et al. [11] utilized a convolutional neural network (CNN) for capacity and RUL prediction, both relying on experimentally measured capacity data. Another approach involves employing ML and DL methods such as Gaussian process regression (GPR) [12], CNN [8,13], and LSTM [14] to extract health-related features from cycling data. These features are then utilized to estimate battery health and RUL. Although these methods can achieve high accuracy with sufficient data, they are limited by the lack of physical interpretability in the design parameters and the sensitivity to noise and disturbances.

The hybrid methods involve the integration of multiple techniques to leverage the strengths of different methods, thereby achieving higher accuracy and robustness. The hybrid of dual data-driven methods and the combination of model-based and data-driven methods are the mainstream hybrid models for predicting the capacity and RUL of LiBs [14]. The hybrid of dual data-driven methods takes advantage of diverse data-driven methods to enhance feature extraction ability and overall performance. For instance, Zhao et al. [15] proposed a framework utilizing both a broad learning system algorithm and LSTM for capacity and RUL prediction. Ren et al. [16] extracted health-related features using CNN and LSTM, and then predicted RULs of LiBs. Some advanced methods, such as self-attention [17] and transformer models [18,19] are combined with other ML and DL methods to predict RULs. The combination of model-based and data-driven methods incorporates the model-based techniques to enhance the physical meanings of the data-driven methods and improve their robustness. For example, Hong et al. [4] and Catelani et al. [20] integrated the filtering-based techniques with data-driven methods for RUL predictions, ensuring the optimized performance of the data-driven methods. To enhance the generality of the data-driven model, Xu et al. [21] proposed a hybrid method based on electrochemical models, enabling early predictions using only 20% of the total data.

Although these methods have achieved promising prediction results, error accumulation exists in the aging trajectory methods, impacting the long-term prediction performance.

For real-world applications, it is challenging to obtain cycling data, especially for metrics like SOH that require fully charged or discharged states during normal use. Based on such limited data, the aforementioned aging trajectory prediction methods, which heavily rely on historical data, may not be suitable for RUL prediction in practical scenarios. To overcome this limitation, aging trajectory prediction methods need to be capable of predicting the aging trajectory starting at the early cycle and making accurate long-term predictions. Nevertheless, the accumulated errors in the multi-step ahead predictions may cause the predicted outcome to deviate significantly from the true aging process [10,22]. Consequently, researchers have developed methods to enhance the long-term prediction ability of the aging trajectory prediction method. For example, Lu et al. [23] and Jones et al. [24] have found that considering future charging/discharging policies in the aging trajectory prediction model can lead to improved long-term prediction. However, obtaining precise future discharging policies is difficult, as discharging policies during usage are often changeable.

Moreover, the capacity regeneration phenomenon (CRP), which is a common phenomenon in the real-world aging trajectory, is ignored in the above aging trajectory prediction methods. In practical scenarios, batteries experience a gradual capacity decline over time due to repeated usage. However, during periods of rest, the electrochemical performance of the battery may temporarily recover, leading to the occurrence of CRP [25]. Ignoring CRP in the long-term capacity predictions can result in error accumulation and adversely affect the accuracy of prediction results [26,27]. Therefore, accurately determining the capacity regeneration point holds significant importance in aging trajectory prediction methods. Zhang et al. [27] utilized an unscented particle filter-Wilcoxon algorithm, and Russell et al. [28] proposed a composite Poisson process for CRP detection. Following CRP detection, the CRP and global degradation are combined to improve RUL prediction accuracy. Additionally, existing researches indicate a strong correlation between CRP and the rest time (t^{rest}) of the battery, with CRP tending to occur after a rest period of more than two hours [29,30]. Qin et al. [30] established a relationship between t^{rest} and CRP using Gaussian processes to predict the global trend. Cui et al. [31] employed support vector regression (SVR) to predict the regeneration amplitude based on t^{rest}, followed by LSTM-based prediction of the entire aging trajectory. Although considering CRP in the modeling process can mitigate a portion of the error accumulation associated with CRP, these methods still need an enhancement in long-term prediction ability.

These challenges motivate us to find practical physical features related to SOH that can improve the long-term prediction accuracy of aging trajectory prediction methods. Additionally, the methods should be transferable to meet the variable usage conditions of LiBs while still retaining their long-term prediction capability.

1.2. Contributions

To address the challenges mentioned above, it is crucial to reduce error accumulation. In this study, two physical enhancement features are introduced to mitigate the error accumulation in the multi-step ahead predictions. Firstly, the future features related to SOH are incorporated to correct predicted aging trajectories. Specifically, the use of R is explored, since it is closely associated with the growth of the SEI layer and side reactions leading to capacity decay [32]. By incorporating future R values into the model, the error accumulation in SOH prediction can be partially corrected. Secondly, t^{rest} is included in the model as an input to detect CRP occurrences and predict the regeneration amplitude. Considering t^{rest} can further improve prediction accuracy. Additionally, the pre-trained model can be fine-tuned to ensure its transferability to different batteries while maintaining long-term prediction ability.

This paper proposes a transferable hybrid method to predict the long-term aging trajectories and RULs of LiBs with CRP. The main contributions of this work can be summarized as follows:

(1) To achieve long-term multi-step ahead SOH and RUL predictions, the proposed hybrid method incorporates two physical enhancement features. The proposed method utilizes not only SOH as inputs but also includes future R and t^{rest} as part of the inputs to make accurate long-term predictions, as well as CRP predictions. Incorporating R and t^{rest} helps eliminate error accumulation in the multi-step ahead prediction.
(2) The transfer learning strategy is utilized to apply the proposed method to batteries tested under various operating conditions. Specifically, the fine-tuning technique is employed to enhance the transferability of the pre-trained model while maintaining its long-term prediction ability.
(3) The proposed method is validated on three LiB degradation datasets that cover different battery types and working conditions. Validation results demonstrate that the proposed method achieves high accuracy in the long-term aging trajectory predictions using only the first 20 cycles' data (approximately 5% of the complete data) as inputs. Furthermore, the model demonstrates high transferability in LiBs under various working conditions and types.

1.3. Article organization

The remainder of this paper is organized as follows. Section 2 presents the definitions and the battery dataset used in this study. Section 3 discusses related algorithms and the proposed prediction framework. The test results of the proposed method are presented in Section 4, followed by a discussion in Section 5. Finally, we draw the conclusions and future work in Section 6.

2. Datasets

2.1. The definitions

The SOH is a measure of a battery's degradation, which can be defined in various ways, such as battery capacity, R, or cycle number [33]. In this work, the capacity ratio is employed as the SOH metric, as defined by Eq. (1):

$$SOH_i = \frac{C_i}{C_0} \times 100\%, \tag{1}$$

where C_i represents the capacity of the battery in the ith cycle, Ah; while C_0 denotes the initial capacity of the battery, Ah. A battery's EOL is typically defined as the cycle number at which its SOH drops below 80%.

The RUL of batteries proposed in this work can be defined as the number of remaining useful cycles in batteries at a specific cycle. RUL in the ith cycle can be computed using Eq. (2):

$$RUL_i = N_{\mathrm{EOL}} - N_i, \tag{2}$$

where N_{EOL} denotes the cycle number at which a battery is considered to have reached its EOL. Additionally, N_i represents the cycle number of the ith cycle.

The rest time here is defined as the time LiBs are left to rest before the next charge cycle. Rest time has a significant impact on the performance and health of LiBs, affecting factors such as CRP and cycle life, which can be represented using Eq. (3):

$$t_i^{\mathrm{rest}} = t_i^{\mathrm{Chgbeg}} - t_{i-1}^{\mathrm{Dchend}}, \tag{3}$$

where t_i^{rest} denotes the rest time of the ith cycle, h. t_i^{Chgbeg} and $t_{i-1}^{\mathrm{Dchend}}$ respectively represent the times at which the ith charge begins and the $(i-1)$th discharge ends, h.

R is an important parameter that reflects the battery's aging performance and is related to the SOH. It is defined as the direct current internal resistance in the charging process, as shown in Eq. (4):

$$R = \frac{(V_2 - V_1)}{I}, \tag{4}$$

where V_2 and V_1 are the voltage values during charging at different times, and I represents the current value during the charging process. R_i denotes the direct current internal resistance in the ith cycle, Ohm. The relative change in R between two adjacent cycles of the battery is defined by the expression $\frac{R_i - R_{i-1}}{R_{i-1}}$, which provides an indicator of how the battery's R changes over cycles.

2.2. Datasets of lithium-ion batteries

In this work, three cyclic test datasets of LiBs with different rated capacities and manufacturing processes are utilized. Two of these datasets, named Dataset CS and Dataset CX, were acquired from the Center for Advanced Life Cycle Engineering (CALCE) at the University of Maryland [34,35]. Both datasets were generated using the Arbin battery tester at room temperature. The third dataset, named Dataset INR18650, comprises Samsung INR18650-25R batteries tested on the Neware battery tester at room temperature.

During the testing process, the batteries in the three datasets were charged following the constant-current constant-voltage (CCCV) charging policy, with a maximum voltage of 4.2 V and a cut-off current of 50 mA. Discharging was performed at a constant-current (CC) rate until the battery reached its minimum voltage. Table 1 provides detailed information on the battery number, rated capacity, and charge/discharge current for each dataset. Batteries in the Dataset INR18650 were charged in fast charging/discharging policies and shelved with different rest times and intervals. INR18650_1 and INR18650_2 underwent repeated rest times and intervals, respectively. The remaining batteries in this dataset followed specific fixed rest times (12 or 24 h) and intervals (10, 20, or 40 cycles) during the whole aging process. The details of the rest times and intervals of Dataset INR18650 are listed in Supplementary Table S1.

Table 1
Summary of the three datasets.

Dataset	Battery	Rated capacity	CC/CV during charge	Discharge current
CS	CS35	1.1 Ah	0.5 C/50 mA	1 C
	CS36	1.1 Ah	0.5 C/50 mA	1 C
	CS37	1.1 Ah	0.5 C/50 mA	1 C
CX	CX34	1.35 Ah	0.5 C/50 mA	0.5 C
	CX36	1.35 Ah	0.5 C/50 mA	0.5 C
	CX37	1.35 Ah	0.5 C/50 mA	0.5 C
	CX38	1.35 Ah	0.5 C/50 mA	0.5 C
INR18650	INR18650_1	2.5 Ah	4 C/50 mA	4 C
	INR18650_2	2.5 Ah	4 C/50 mA	4 C
	INR18650_3	2.5 Ah	4 C/50 mA	4 C
	INR18650_4	2.5 Ah	4 C/50 mA	4 C
	INR18650_5	2.5 Ah	1 C/50 mA	4 C
	INR18650_6	2.5 Ah	1 C/50 mA	4 C
	INR18650_7	2.5 Ah	4 C/50 mA	1 C
	INR18650_8	2.5 Ah	4 C/50 mA	1 C

Fig. 1 illustrates the SOH aging trajectories of three datasets. It is worth noting that the SOH does not exhibit a steady decay during the aging process. CRP exists during cycling, and t^{rest} is related to the CRP during this process [30,36]. Fig. 2 shows the impact of t^{rest} and SOH on the capacity regeneration amplitude (detailed in Supplementary Note 2). This figure demonstrates that larger t^{rest} and SOH may result in a greater capacity regeneration amplitude. This regeneration phenomenon arises from the dissipation of reactants in the battery during static states [15]. With increasing t^{rest} and SOH, the amount of reactant dissipation also rises, leading to a higher capacity recovery. As a result, these datasets are well-suited for real-world trajectory prediction techniques to accurately predict aging trajectories with CRP.

2.3. Experiment scenarios

To evaluate the proposed method in long-term predictions and the transferability, four scenarios are selected as follows:

Scenario 1: The Dataset CS, Dataset CX, and four batteries (INR18650_1-4) in Dataset INR18650 are selected to evaluate the long-term prediction performance of the proposed method.

Scenario 2: Four batteries (INR18650_1-4) and the other two batteries (INR18650_5, 6) in Dataset INR18650 are selected as Scenario 2 to evaluate model transferability on batteries with different charging policies.

Scenario 3: Four batteries (INR18650_1-4) and the other two batteries (INR18650_7, 8) in Dataset INR18650 are selected to evaluate model transferability on batteries with different discharging policies.

Scenario 4: The Dataset CS and Dataset CX are used to evaluate model transferability on batteries with different types.

3. Proposed method

This study proposes two models: the R prediction model and the SOH trajectory prediction model. The R prediction model applies CNN to forecast the R of LiBs. Meanwhile, the SOH trajectory prediction

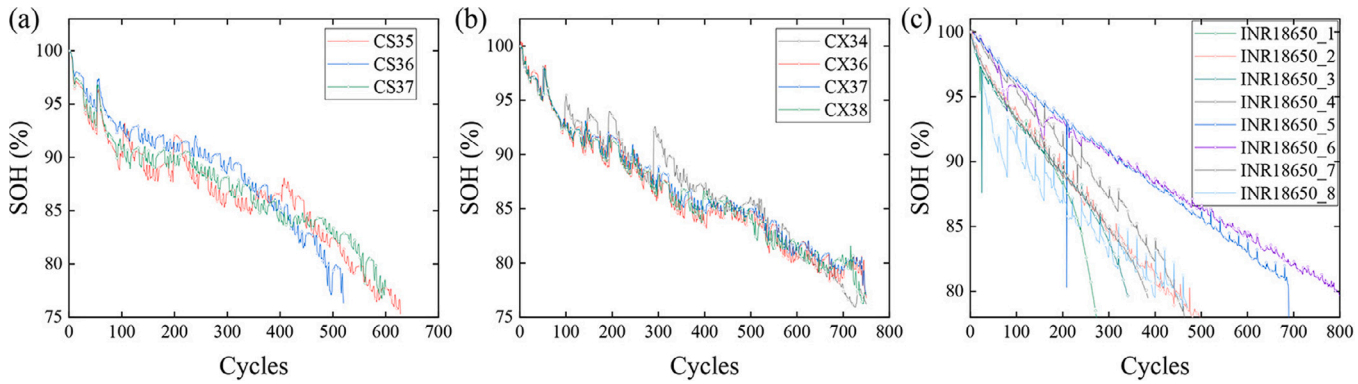

Fig. 1. The SOH aging trajectories. (a) Dataset CS. (b) Dataset CX. (c) Dataset INR18650.

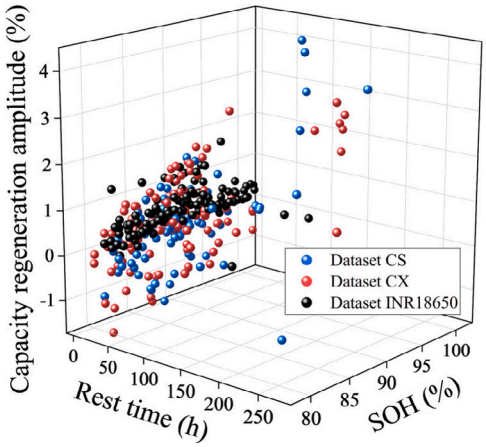

Fig. 2. The impact of rest time and SOH on the capacity regeneration amplitude.

model combines CNN, dilated CNN, and LSTM to predict the aging trajectories and RULs of LiBs. Specifically, CNN and dilated CNN are employed to extract features from a sequence of cycling data, while LSTM networks are utilized to learn the degradation mechanism of these features over cycles. The extracted features from CNN, dilated CNN, and LSTM are then processed through a fully connected (FC) layer, which outputs the predicted SOH.

3.1. Related algorithms

3.1.1. CNN and dilated CNN algorithm

The main concept of CNN is to intelligently adapt to the properties and extract features from input data by utilizing multiple filters [37]. In this paper, one-dimensional convolution in the time domain is employed to extract features from the input data. The convolution process in each layer of the network can be represented as Eq. (5):

$$Z_n^{l,r} = f(K^{l,r} \cdot O^{l-1}(n) + b^{l,r}), r = 1, 2, \ldots, k^l, \tag{5}$$

where O^{l-1} represents the output of layer $l-1$, $O^{l-1}(n)$ denotes the nth subvector of O^{l-1}, k^l denotes the kernel number in the lth convolutional layer, vector $K^{l,r}$ and $b^{l,r}$ represent the weights and biases of the rth kernel in the lth convolutional layer. The activation function $f(\cdot)$ used here is the rectified linear unit (ReLU) function. Additionally, $Z_n^{l,r}$ denotes the nth subvector of the outputs of the lth convolutional layer in the rth kernel.

To prevent overfitting and reduce the number of model parameters, a max pooling technique is applied after two convolutional layers. This operation can be expressed mathematically as Eq. (6):

$$MP_m = \max_{[(m-1)\times s+1] \le i \le [p+(m-1)\times s]} (Z_i^2), \tag{6}$$

where s and p are the stride and pool size of the max pooling layer, MP_m denotes the mth subvector of outputs of the max pooling layer, Z_i^2 is the ith subvector of the outputs of the 2nd convolutional layer.

The CNN block typically consists of several convolutional and max pooling layers. However, pooling layers can lead to the loss of information due to down-sampling. To address this issue, dilated CNN is employed. This technique utilizes dilated convolution, which can apply filters with different dilation rates and increase the area that the filter covers [38,39]. The structures of CNN and dilated CNN are illustrated in Supplementary Fig. S19.

Generally, the feature maps from the last layer are commonly fed into an FC layer in CNN. Nonetheless, using this FC layer may lead to overfitting and consequently decrease the network's ability to generalize [40]. To address these issues, the global average pooling (GAP) layer is employed in place of the FC layer in both CNN and dilated CNN blocks. The GAP mechanism calculates the mean value of each feature map, thereby reducing the network's parameters and enhancing its generalization performance.

3.1.2. LSTM algorithm

The LSTM is a form of recurrent neural network (RNN) that addresses the vanishing gradient problem by utilizing memory cells and gates to regulate the flow of information. This feature enables it to effectively capture long-term dependencies in time series data [41,42]. The structure of LSTM is shown in Supplementary Fig. S20. The LSTM layer includes three gates: the forget gate, the input gate, and the output gate.

Forget gate. The forget gate decides how much information from the previous moment is going to be thrown away. The forget gate is described as Eq. (7):

$$f_t = \sigma(W_f \cdot [h_{t-1}, X_t] + b_f), \tag{7}$$

where f_t represents the output of forget gate. It is a number between 0 and 1, where 1 signifies a fully retained state value, and 0 signifies a fully forgotten state value. Additionally, h_{t-1} denotes the hidden state at the previous moment $t-1$, X_t is the input vector at time t. W_f and b_f are the weights and biases of the forget gate. Besides, "[]" is vector concatenation, and $\sigma(\cdot)$ represents the sigmoid activation function.

Input gate. The input gate determines what new information will be updated, which can be expressed as Eqs. (8) and (9):

$$i_t = \sigma(W_i \cdot [h_{t-1}, X_t] + b_i), \tag{8}$$

$$\tilde{C}_t = \tanh(W_c \cdot [h_{t-1}, X_t] + b_c), \tag{9}$$

where $[W_i, b_i]$ and $[W_c, b_c]$ represent the input gate's and candidate vector's weights and biases, respectively. i_t signifies the output of the input gate, $\tilde{C}_t$ denotes a vector of the candidate state at time t. Additionally, $\tanh(\cdot)$ refers to the tanh activation function.

Then the previous state C_{t-1} can be updated to the current state C_t by combining Eqs. (7)–(9), as shown in Eq. (10):

$$C_t = f_t \times C_{t-1} + i_t \times \tilde{C}_t. \tag{10}$$

Output gate. The output gate determines the final output of LSTM. The output gate can be implemented as Eqs. (11) and (12):

$$o_t = \sigma(W_o \cdot [h_{t-1}, X_t] + b_o), \tag{11}$$

$$h_t = o_t \times \tanh(C_t), \tag{12}$$

where W_o and b_o are the weights and biases of the output gate, respectively. o_t is the output of the output gate, and h_t is the final output.

3.1.3. Proposed method based on transfer learning

Transfer learning is a powerful technique that enables the sharing of learned knowledge between related tasks, thereby avoiding the need to learn a new task from scratch. In the context of aging trajectory prediction, transfer learning can be especially valuable as it allows information from the source data to be leveraged by the target task, reducing the need for large amounts of training data [43].

However, predicting the aging trajectories of batteries tested under different conditions presents unique challenges, as the degradation patterns may vary between batteries. To address this challenge, we propose a novel transfer learning method that can be applied to different batteries, leveraging the long-term degradation patterns of the SOH and R values. Specifically, we only fine-tune the FC layers of the SOH trajectory prediction model and the R prediction model. The transfer learning approach is shown in Supplementary Fig. S21. By fine-tuning only the FC layers, the learned knowledge can be effectively transferred from the source domain to the target domain while avoiding overfitting the specific characteristics of the source data, thus maintaining the long-term prediction ability.

3.2. Framework

3.2.1. The network architectures of two models

The network architectures of the two proposed models are shown in Fig. 3. The R prediction model utilizes a CNN block comprising multiple CNN layers to model the behavior of R changes. Depending on the scenario, the input length of the R prediction model varies. Specifically, in Scenarios 1–3 and Scenario 4, the input lengths are set to 20 and 40 cycles, respectively. The R prediction model can forecast future R values with a flexible length until the EOL is reached.

As illustrated in Fig. 3, the SOH trajectory prediction model considers SOH_i, t_{i+1}^{rest}, R_{i+1}, and $\frac{R_{i+1}-R_i}{R_i}$ during 20 consecutive cycles as inputs. The inclusion of R_{i+1} and $\frac{R_{i+1}-R_i}{R_i}$ helps the model to capture the changes from SOH_i to SOH_{i+1} and reduces the error accumulation during long-term forecasting. Additionally, t_{i+1}^{rest} is used to predict whether CRP occurs in the (i+1)th cycle, allowing for CRP predictions. The outputs of the GAP and LSTM layers are fed into a FC layer, which predicts the SOH of the next cycle. During the transfer learning process, only the FC layers are fine-tuned.

3.2.2. Implementation process

The process of implementing the RUL prediction method with all algorithms is illustrated in Fig. 4. It can be divided into the following three main parts. First, in offline training, the R prediction model and the SOH trajectory prediction model are trained on the source dataset. Then, the two models are fine-tuned to enhance their transferability to batteries different from those in the source dataset in offline transfer learning. At last, these two models are employed to forecast the future aging trajectory and RUL of the target battery.

(1) **Offline training.** During the offline training process, the R prediction model and SOH trajectory prediction model are trained by minimizing the mean squared error (MSE) loss between model outputs and targets on the training set. The R prediction model uses the R values during the first M cycles as input and predicts the future R until EOL. The cycle data of LiBs in the training set are divided into numerous samples, where each sample includes an input matrix of SOH_i, t_{i+1}^{rest}, R_{i+1}, and $\frac{R_{i+1}-R_i}{R_i}$ during 20 consecutive cycles, and a target matrix of SOH_{i+20}. Subsequently, the SOH trajectory prediction model is trained on these samples.

(2) **Offline transfer learning.** For Scenario 1, transfer learning is not used because the source dataset and the target battery have the same charging/discharging policies and types. Scenarios 2 and 3 have the same battery type, but the charging/discharging policies of the source dataset and target battery are different. In this situation, transfer learning is required for the SOH trajectory prediction model. For Scenario 4, the types of the source dataset and target battery are different. Both the R prediction model and SOH trajectory prediction model are transferred by fine-tuning the model parameters. Specifically, the R prediction model is fine-tuned on batteries of the same type as the target battery. The SOH trajectory prediction model is fine-tuned using the first 40 cycles' data from the target battery. The transfer learning process for the SOH trajectory prediction model involves two steps: first, a dataset containing 20 samples is created by using a sliding window with a size of 20 and a step of 1 in the first 40 cycles' data of the target battery. Second, the fine-tuning process focuses solely on the MSE loss in this dataset and does not validate the future trajectory of the target battery. Once completed, the fine-tuned SOH trajectory prediction model can be applied to the target battery. The detailed descriptions of the transfer learning process of different scenarios with examples are shown in Supplementary Note 4.

(3) **Online deployment.** Once the models are trained and fine-tuned, they are ready for online deployment. Given the first M cycles' data of the target battery, the R prediction model directly outputs the predicted future R values. These predicted R values are then used as inputs for the SOH trajectory prediction model, which generates multi-step SOH predictions with a sliding window of 20 cycles until EOL is reached.

In Scenario 1, both the training and test batteries are selected from the same dataset. In Scenarios 2 and 3, the training batteries consist of INR18650_1–4, with INR18650_5, 6, and INR18650_7, 8 used as the test batteries for Scenarios 2 and 3, respectively. For Scenario 4, the proposed method is applied using Dataset CX as the training set and Dataset CS as the test set. In Scenarios 1–3, the value of M is set to 20, while for Scenario 4, M is set to 40.

3.2.3. Evaluation index

To evaluate the performance of the proposed method in RUL prediction, two indexes are selected: (1) the RUL error, as described in Eq. (13), which quantifies the discrepancy between the true RUL and the predicted RUL; and (2) the accuracy metric (AM), as expressed in Eq. (14), which assesses the accuracy of the models.

$$RUL_{\text{Error}} = \widehat{RUL} - RUL, \tag{13}$$

$$AM = (1 - \frac{|RUL_{\text{Error}}|}{RUL}) \times 100\%, \tag{14}$$

where RUL and $\widehat{RUL}$ represent the actual RUL and the predicted RUL, respectively. In these metrics, the larger AM is, and the smaller RUL_{Error} is, the higher the accuracy of the proposed model is.

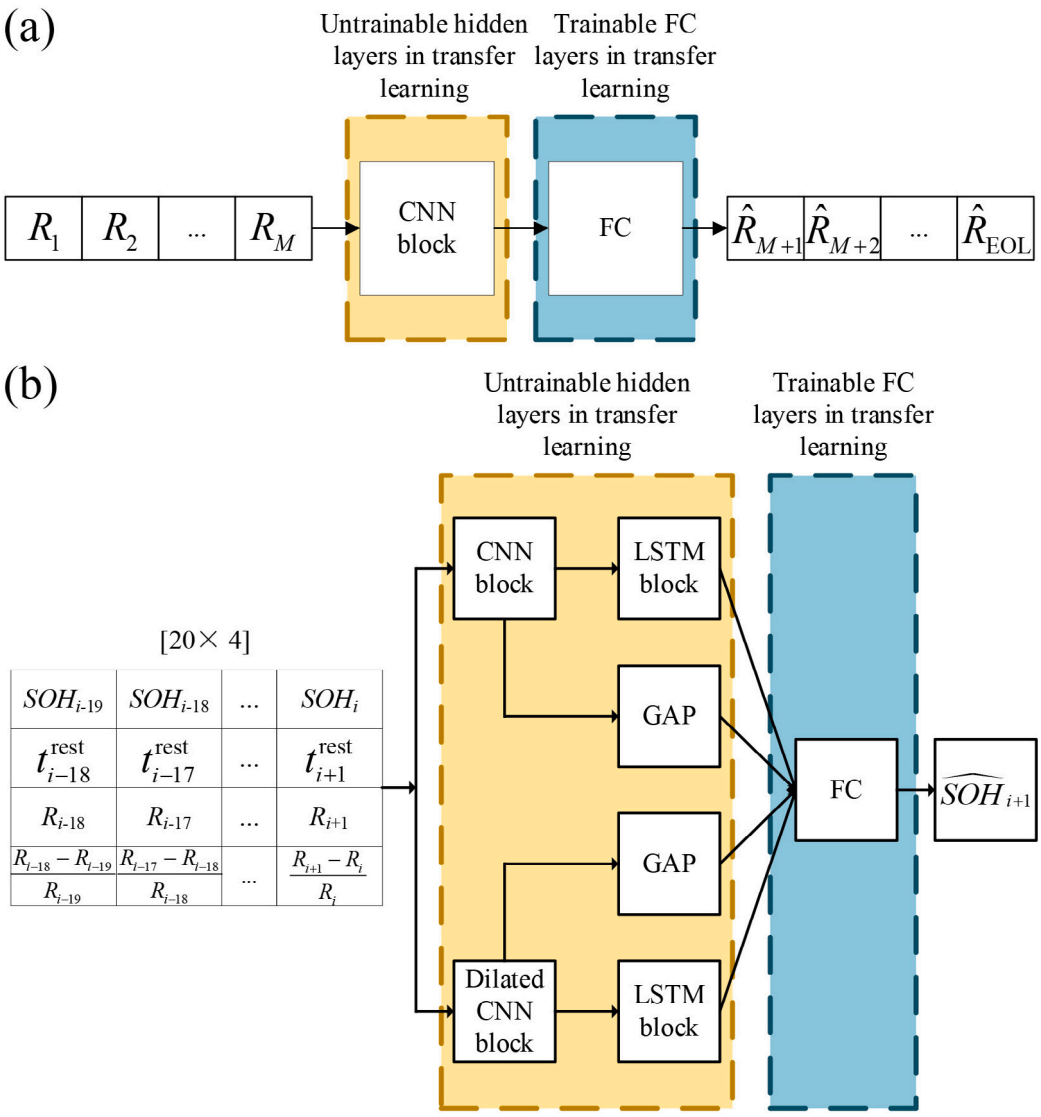

Fig. 3. The network architectures of the proposed two models. (a) R prediction model. In Scenarios 1–3, M is set to 20, while in Scenario 4, M is set to 40. (b) SOH trajectory prediction model. The ˆ notation denotes the predicted value.

4. Estimation results

4.1. Experiment design

In this section, we verify the performance of the proposed method for predicting RULs. In Section 4.2, the method is trained and evaluated on three different datasets. Section 4.3 compares the proposed method with a model that only uses SOHs as inputs to evaluate whether including R and t^{rest} improves the accuracy of the CRP estimate and the long-term prediction performance. Subsequently, comprehensive tests are carried out to assess the transferability of the proposed method to batteries tested under different conditions. Batteries with different charging/discharging policies and types are tested in Sections 4.4.1 and 4.4.2, respectively.

4.2. The prediction results of three datasets using the proposed method

The proposed method is used to estimate aging trajectories and predict RUL using historical data from batteries in Scenario 1. In this experiment, each battery was chosen as the test set, while the remaining batteries in the dataset were used as the training set. The degradation data of the batteries in the training set were used to train the models. Subsequently, the first 20 cycles' data of the test set were used for SOH trajectory and RUL predictions. The prediction process was terminated when the predicted SOH dropped below 80%, and the predicted RUL was obtained at that point.

The R and SOH trajectory prediction results for batteries in Scenario 1 are presented in Fig. 5, Supplementary Fig. S5, and Supplementary Fig. S6. From Fig. 5(a–c), Fig. S5(a–d), and Fig. S6(a–d), it can be observed that the R prediction model performs well on test batteries. The model can capture the R-related trends during the battery's entire lifespan because it can learn R-related features from the batteries in the training set. Moreover, Fig. 5(d–f), Fig. S5(e–h), and Fig. S6(e–h) show that the SOH trajectory estimations of the proposed method can fit the real SOH curves well. Additionally, the SOH trajectory prediction model can estimate the SOH value for over 300 cycles using only the first 20 cycles' data, indicating that considering R and t^{rest} improves the long-term prediction performance of the SOH trajectory. Table 2 lists the numeric results, demonstrating that the proposed method can accurately and robustly predict RUL with AMs larger than 95% in Dataset CS and Dataset CX. For fast charging conditions, AMs of Dataset INR18650 are all larger than 92% based on the data from the first 6% of the whole life. The AMs of Dataset INR18650 are smaller than those of Dataset CS and Dataset CX, mainly because the batteries in Dataset INR18650 are

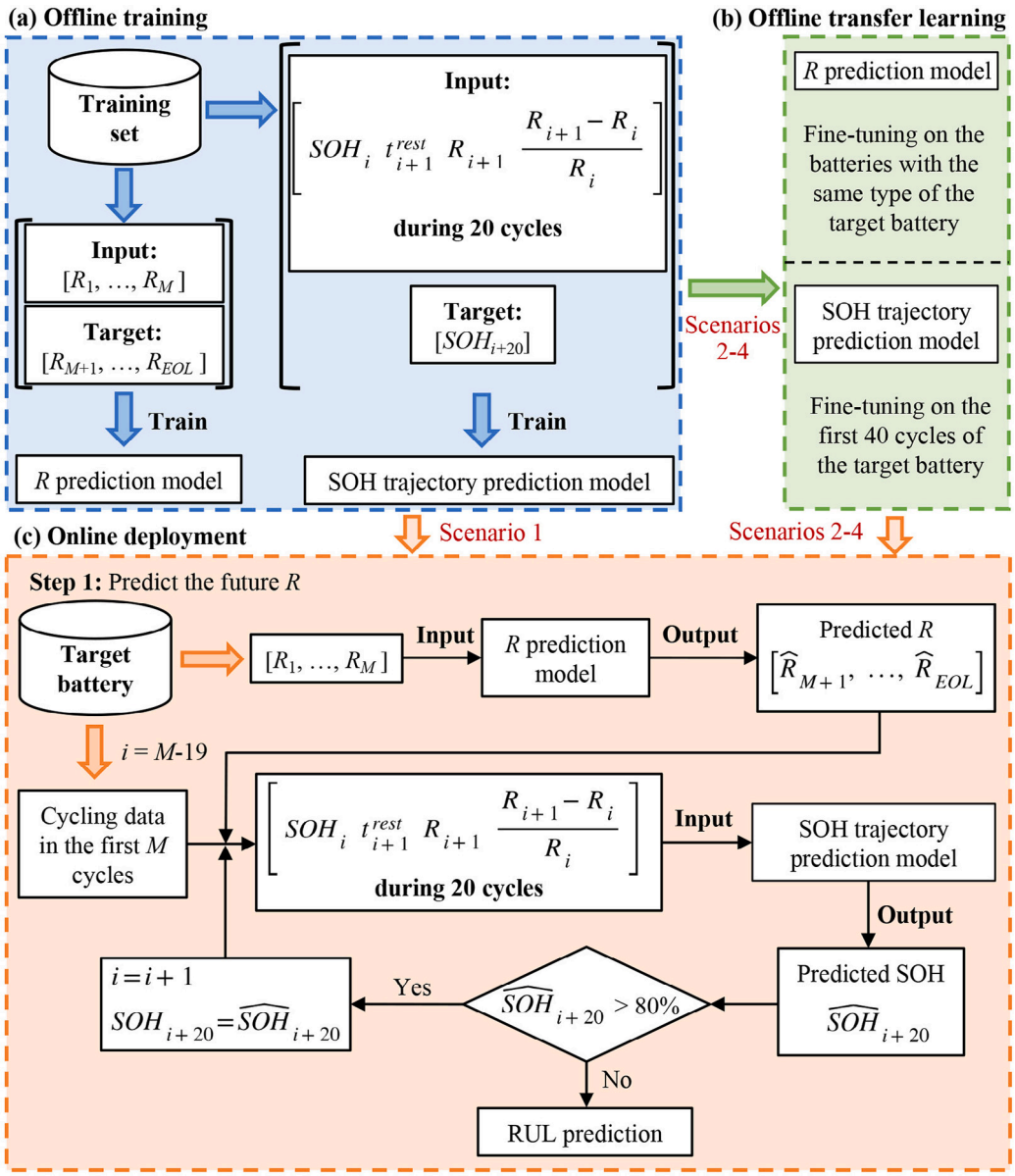

Fig. 4. The implementation process of the proposed method. (a) Offline training process. (b) Offline transfer learning process. Scenario 1: same charging/discharging policies and battery types; Scenarios 2–4: different charging/discharging policies or battery types. (c) Online deployment process. The ˆ means the predicted value.

tested in the laboratory, and the rest times and intervals are manually set. The rest times and intervals of Dataset INR18650 shown in Table S1 indicate that there exist two main problems: (1) the rest times and intervals of each battery are different from the other batteries. (2) The rest times and intervals are insufficient. Therefore, it is challenging for the SOH trajectory prediction model to learn enough information from the training set to ensure model generality on unseen rest times and intervals. As a result, the proposed method does not perform well in Dataset INR18650. Compared to Dataset INR18650, Dataset CS and CX are more suitable to evaluate the model's performance since the aging trajectories in Dataset CS and CX are more realistic.

Table 2
RUL prediction results of the proposed method for Scenario 1.

Dataset	Train on	Test on	RUL	$\widehat{RUL}$	Error	AM
CS	CS36, 37	CS35	510	533	23	95.49%
	CS35, 37	CS36	466	456	−10	97.85%
	CS35, 36	CS37	534	518	−16	97.00%
CX	CX36, 37, 38	CX34	615	625	10	98.37%
	CX34, 37, 38	CX36	614	607	−7	98.86%
	CX34, 36, 38	CX37	629	614	−15	97.62%
	CX34, 36, 37	CX38	602	604	2	99.67%
INR18650	INR18650_2, 3, 4	INR18650_1	245	262	17	93.06%
	INR18650_1, 3, 4	INR18650_2	401	369	−32	92.02%
	INR18650_1, 2, 4	INR18650_3	318	294	−24	92.45%
	INR18650_1, 2, 3	INR18650_4	360	344	−16	95.56%

4.3. The prediction results using only SOHs as input

To further verify the accuracy of the proposed approach, we developed a model that only utilizes SOHs as inputs to predict the aging trajectory of Dataset CS. The results of this model's predictions are presented in Fig. 6. The findings indicate that the model performs well in the short term, but its performance significantly declines when attempting long-term multi-step ahead predictions due to the existence of the error accumulation [44]. For instance, when employing a SOH trajectory prediction model that only relies on SOHs, the model's capability to forecast the SOH is limited to previous SOH values. As

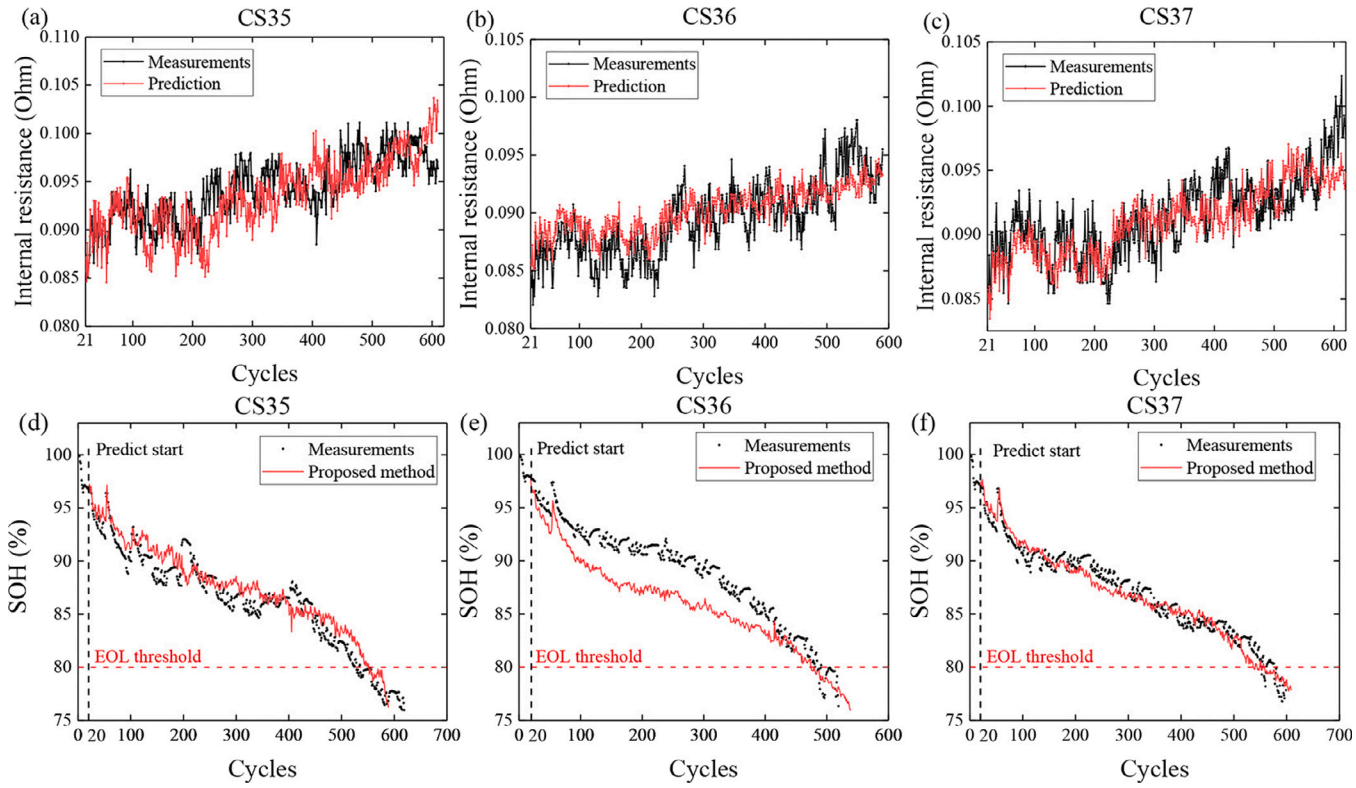

Fig. 5. *R* prediction (a–c) and SOH trajectory prediction (d–f) of CS35, CS36, CS37. The training set of each battery is the rest batteries in Dataset CS.

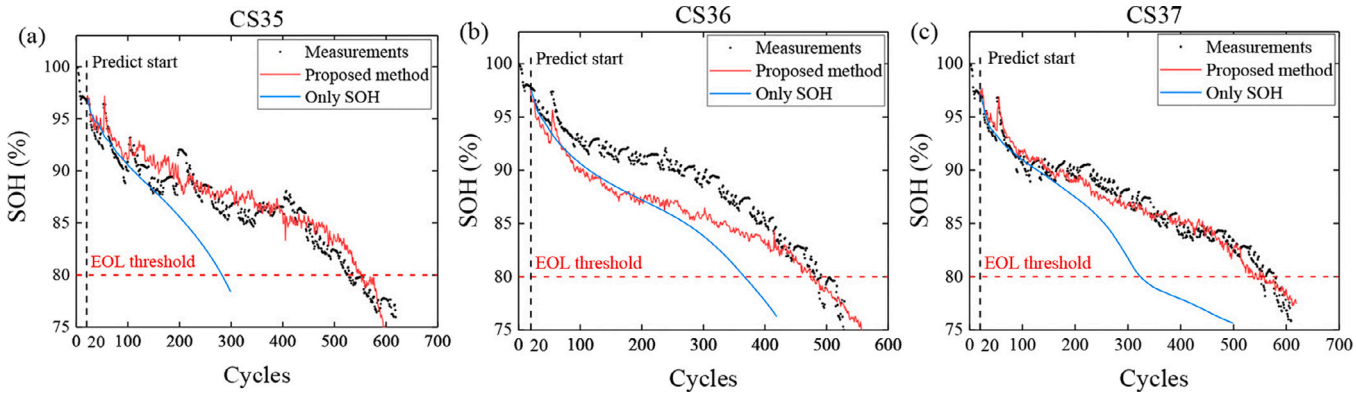

Fig. 6. SOH trajectory prediction using only SOHs as input. (a) CS35. (b) CS36 (c) CS37.

a result, if all SOHs in the sliding window are predicted values, the estimated SOH in the next cycle may be influenced by prior forecast errors, resulting in cumulative errors that considerably impair long-term forecasts. By incorporating *R* and t^{rest}, the proposed hybrid method can achieve long-term forecasts of aging trajectory. *R* is correlated with SOH and can eliminate part of the error accumulation, thereby leading to more accurate SOH trajectory predictions. The inclusion of t^{rest} helps predict the CRP and enhances prediction accuracy.

4.4. Model transferability of the proposed method

In this section, the model transferability of the proposed method is tested and discussed. As discussed in Section 4.3, the long-term prediction is not accurate when only considering the SOHs, thus the transferability of the aging trajectory prediction model using only SOHs is not evaluated in this work.

4.4.1. Model transferability on batteries with different charging/discharging policies

In this section, Scenarios 2 and 3, including batteries with different charging/discharging policies, have been chosen to verify the ability of the transfer learning method on such batteries. The fine-tuning process is shown in Section 3.2.2.

The SOH trajectory prediction results demonstrate the effectiveness of the proposed transfer learning method in correcting predicted SOH trajectory values to measured values, as shown in Fig. 7 and Table 3. Supplementary Fig. S8 shows that although the charging/discharging policies differ, the *R* prediction model can still evaluate the *R* trends well without fine-tuning. It indicates that the *R* patterns can be captured by the *R* prediction model on the same battery type since the *R* trajectories in Scenario 2 and Scenario 3 are similar to Scenario 1. As can be seen in Fig. S8, when the *R* trajectories are close to their EOLs, the predictions are not particularly accurate, mainly because the battery life in the training set is too short for the model to learn

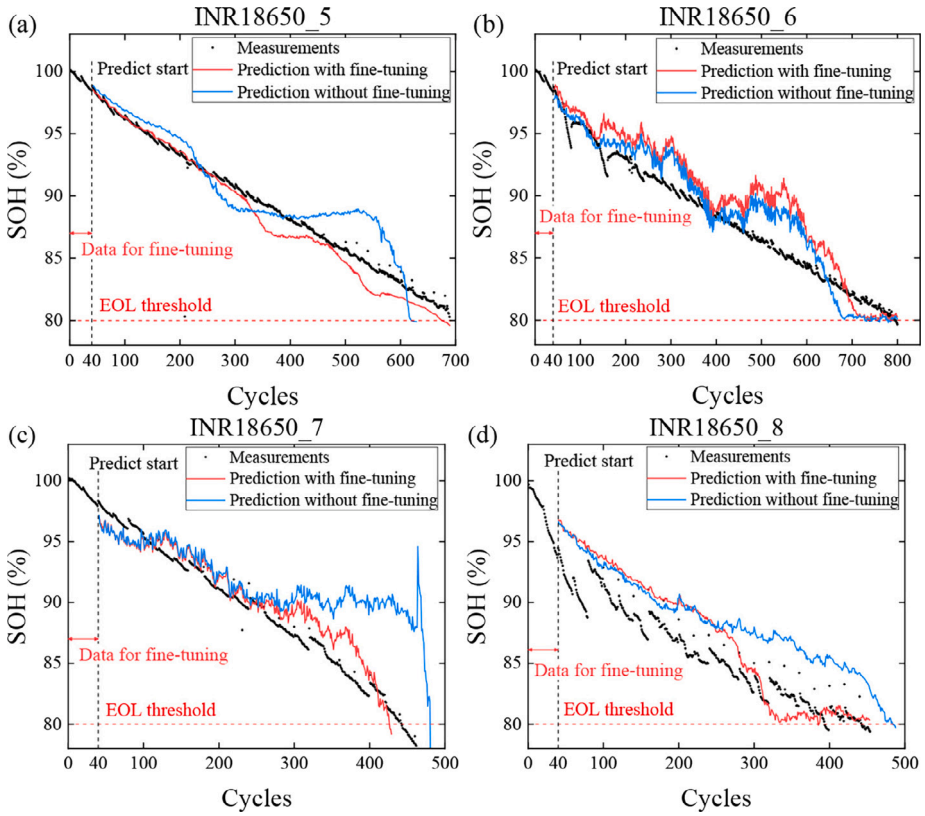

Fig. 7. SOH trajectory prediction results for batteries with different charging/discharging policies. (a) INR18650_5. (b) INR18650_6. (c) INR18650_7. (d) INR18650_8. The batteries in the training set are INR18650_1-4.

Table 3
RUL prediction results of Scenario 2 and 3.

Train on	Scenario	Fine-tuning and test on	RUL	Fine-tuning	$\widehat{RUL}$	Error	AM
INR18650_1-4	2	INR18650_5	649	No	579	−70	89.21%
				Yes	635	−14	97.84%
		INR18650_6	755	No	688	−67	91.13%
				Yes	721	−34	95.50%
	3	INR18650_7	403	No	441	38	90.57%
				Yes	387	−16	96.03%
		INR18650_8	354	No	444	90	74.58%
				Yes	335	−19	94.63%

the R situation when the number of cycles is large. However, the deep learning model can predict unknown conditions based on the learned characteristics, indicating its potential for generalization and prediction of R for unknown cycles. For Scenario 2, the INR18650_5 and INR18650_6 charge at a lower current rate and have lifetimes of over 600 cycles, which are longer than INR18650_1-4. The proposed method can still estimate the SOH trajectory well and make a relatively high prediction accuracy of more than 90% AM without fine-tuning. After fine-tuning, the AMs of the INR18650_5 and INR18650_6 increase to more than 95%. In Scenario 3, the INR18650_7 and INR18650_8 discharge at a lower current rate than INR18650_1-4, and the aging trajectory of INR18650_8 is completely different from that of other batteries, which makes the prediction more difficult. After fine-tuning, the prediction trajectory is closer to the measurements, highlighting the advantage of the transfer learning method that can fit the pre-trained model to the target battery, with the AMs of 96.03% and 94.63% for INR18650_7 and INR18650_8.

4.4.2. Model transferability on different battery types

To ensure the applicability of the proposed method to batteries with different types, both the R prediction model and SOH trajectory prediction model undergo fine-tuning. The training set is Dataset CX, while Dataset CS is used as test batteries to evaluate the performance of the transfer learning. Detailed information about the fine-tuning process is available in Section 3.2.2.

Supplementary Fig. S9 presents the predicted R of Dataset CS after fine-tuning. The experiment results demonstrate that R can be accurately predicted with the proposed transfer learning method, which helps reduce error accumulation and enhances the accuracy of the SOH trajectory prediction model. Consequently, the proposed method achieves high prediction accuracy, even when the source and target datasets have different battery types. Fig. 8 and Table 4 show the comparison results between the RUL prediction method and the method after fine-tuning. The experiment results exhibit that the pre-trained model accurately predicts the RUL, with AMs of 86.73%, 99.33%, and 94.94% for CS35, CS36, and CS37, respectively. The transfer learning method facilitates the fine-tuning of the pre-trained model on a new dataset, making it more compatible with the new battery. During the fine-tuning process, only the FC layers undergo retraining, implying that only the mapping from latent representations to output is modified. Furthermore, a small learning rate is utilized for fine-tuning the FC layer, leading to a minor change in the learned mapping. Employing

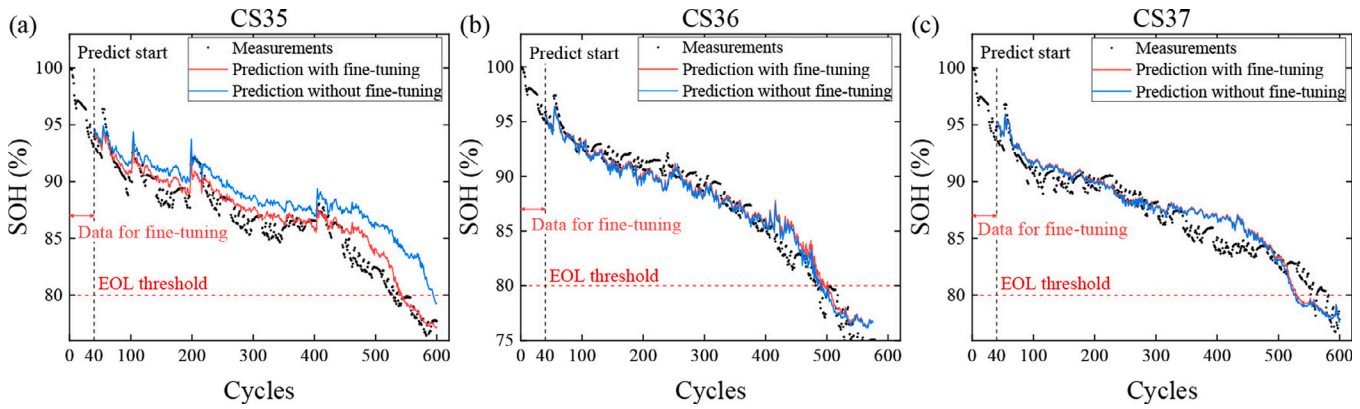

Fig. 8. SOH trajectory prediction results on different battery types. (a) CS35. (b) CS36. (c) CS37.

Table 4
RUL prediction results of Scenario 4.

Train on	Fine-tuning and test on	RUL	Fine-tuning	$\widehat{RUL}$	Error	AM
Dataset CX	CS35	490	No	555	65	86.73%
			Yes	503	13	97.35%
	CS36	446	No	449	3	99.33%
			Yes	456	10	97.76%
	CS37	514	No	488	−26	94.94%
			Yes	489	−25	95.14%

this strategy, the predicted curve aligns better with the actual value, resulting in improved RUL prediction accuracy with AMs larger than 95% for all three batteries. Although the accuracy of the transferred RUL prediction method reduces slightly for CS36, the loss in accuracy is not significant since only the FC layer was fine-tuned.

5. Discussion

The proposed method considers *R* and CRP in LiBs to make long-term aging trajectory and RUL prediction. It has the following advantages:

(1) **High accuracy in long-term prediction.** Due to the consideration of the *R* and CRP, the proposed method can achieve accurate long-term SOH trajectory and RUL prediction. In comparison to existing aging trajectory prediction models, which typically require more than 20% of the entire cycling data for training and predicting, the proposed model can be utilized directly and initiate predictions at the early stage of battery aging. Furthermore, the AMs of the prediction results are 96.78% for Dataset CS, 98.63% for Dataset CX, and 93.27% for Dataset INR18650 in Scenario 1, demonstrating the long-term prediction ability of the proposed method.

(2) **CRP detection.** The proposed hybrid method can predict the CRP occurrence and the amplitude of capacity regeneration in the aging trajectory predictions, making it a suitable method for real-world application.

(3) **Excellent transferability in LiBs with different conditions.** The transfer learning method is employed to make the proposed approach suitable for LiBs tested under various conditions. When the charging/discharging policies of the training set and test set differ, the proposed method can still achieve high AMs of 96.67% and 95.33% by transfer learning for Scenarios 2 and 3, respectively. Transfer learning also demonstrates its ability to adapt the pre-trained model to batteries of different types with the source data, achieving an AM of 96.75%.

(4) **Real-time performance.** We also performed experiments to evaluate the real-time performance, i.e., estimation speed, of our method. Normally, RUL estimation results can be obtained within 10 s. This estimation speed may be sufficient for many real-world applications of RUL prediction. For example, in the situations of predictive maintenance and EVs' BMS, an estimation speed of 10 s is usually enough to meet practical requirements. However, for optimal charging/discharging management and some mission-critical applications, a shorter estimation time can lead to better results. A detailed discussion about the real-time usage of our method is presented in Supplementary Note 11.

(5) **Performance compared with previous relevant works.** Among relevant methods, both Ref. [23] and the proposed hybrid method demonstrate the ability to achieve precise aging trajectory predictions. The advanced early and long-term prediction ability indicates that considering future health-related features can effectively reduce error accumulation in long-term forecasting. Additionally, compared to Ref. [23], the proposed method can predict the CRP in the aging trajectory predictions, which may be more suitable for practical usage. Although the proposed method does not achieve the highest AM among previous works, the results demonstrate the power of the proposed method in achieving a balance between long-term and accurate predictions of the aging trajectory and RUL. A detailed discussion about the comparison of the proposed method and other relevant recent literature is presented in Supplementary Note 12.

The proposed method has the potential to be utilized as an early-stage trajectory and RUL prediction technology in EVs for various applications, owing to its long-term prediction ability. When the proposed method is used in real applications, it may require the following steps after model training. Firstly, the *R* prediction model can be used to predict the future *R* based on the first 20 cycles' *R*, which can be easily obtained before the batteries are used in EVs. After that, the SOH trajectory prediction model can be integrated into the existing BMS to make multi-step ahead SOH predictions directly. These predicted values can assist users in understanding the battery's aging performance. Moreover, the CRP can be calculated using the proposed method. If users want to learn how the rest time value affects the capacity regeneration value, the proposed method can predict the capacity regeneration value following the set rest time. To reduce computational burden and minimize the need for data on batteries under different conditions, the pre-trained model can be applied to other types of LiBs using transfer learning. In the transfer learning process, the *R* curves of new battery types are relatively easy to obtain because manufacturers usually conduct cycling tests to obtain the performance of new battery types. Therefore, the proposed transfer learning process is practical.

Although the proposed model shows high accuracy in long-term SOH and RUL predictions, the datasets used in this work are obtained from laboratory measurements, leading to a large discrepancy with real-world battery data. For instance, the temperature, which is an important influencing factor for LiBs, typically remains constant during laboratory testing, while in real-world applications, the environmental temperature can fluctuate sharply. Consequently, the proposed method may require more training data to accommodate a wider range of real-world situations and a wider range of battery types.

6. Conclusion and future work

This paper presents a transferable LiB aging trajectory prediction method with long-term prediction ability. The proposed hybrid method incorporates two physical enhancement features, R and t^{rest}, to reduce error accumulation in long-term SOH forecasts and achieve accurate long-term SOH and RUL prediction. The experiment results demonstrate that the prediction error is less than 5% for three different datasets when using only the first 20 cycles (approximately 5% of the entire life data). Additionally, the proposed method can detect CRP in the aging trajectory, making it suitable for practical applications. Moreover, the proposed method is transferable to different aging conditions while still maintaining its long-term prediction ability. This work highlights the combination of future physical features with data-driven methods can improve the performance of early and accurate prediction in the aging trajectory.

Future research should investigate the aging mechanism of LiBs in real-world conditions and apply the transfer learning method to a wider range of battery types to verify its feasibility and examine the impact of temperature on SOH trajectory and RUL prediction.

CRediT authorship contribution statement

Yaodi Huang: Writing – original draft, Methodology, Formal analysis. **Pengcheng Zhang:** Writing – review & editing, Formal analysis. **Jiahuan Lu:** Formal analysis. **Rui Xiong:** Writing – review & editing, Project administration. **Zhongmin Cai:** Writing – review & editing, Project administration.

Declaration of competing interest

The authors declare that they have no known competing financial interests or personal relationships that could have appeared to influence the work reported in this paper.

Data availability

The Dataset INR18650 developed in this study is available at https://data.mendeley.com/datasets/56hdnvr7hs.

Acknowledgments

This work was supported by the National Key R&D Program of China (2021YFB2400800, 2021YFB2402002) and Beijing Natural Science Foundation (Grant No. L223013).

Appendix A. Supplementary data

Supplementary material related to this article can be found online at https://doi.org/10.1016/j.apenergy.2024.122825.

References

[1] Zhang Y, Xiong R, He H, Shen W. Lithium-ion battery pack state of charge and state of energy estimation algorithms using a hardware-in-the-loop validation. IEEE Trans Power Electron 2016;32(6):4421–31.
[2] Omariba ZB, Zhang L, Sun D. Review on health management system for lithium-ion batteries of electric vehicles. Electronics 2018;7(5):72.
[3] Schmuch R, Wagner R, Hörpel G, Placke T, Winter M. Performance and cost of materials for lithium-based rechargeable automotive batteries. Nat Energy 2018;3(4):267–78.
[4] Hong S, Qin C, Lai X, Meng Z, Dai H. State-of-health estimation and remaining useful life prediction for lithium-ion batteries based on an improved particle filter algorithm. J Energy Storage 2023;64:107179.
[5] Li Y, Li K, Liu X, Wang Y, Zhang L. Lithium-ion battery capacity estimation—A pruned convolutional neural network approach assisted with transfer learning. Appl Energy 2021;285:116410.
[6] Rauf H, Khalid M, Arshad N. Machine learning in state of health and remaining useful life estimation: Theoretical and technological development in battery degradation modelling. Renew Sustain Energy Rev 2022;156:111903.
[7] Reniers JM, Mulder G, Howey DA. Review and performance comparison of mechanical-chemical degradation models for lithium-ion batteries. J Electrochem Soc 2019;166(14):A3189–200.
[8] Zhou Z, Liu Y, You M, Xiong R, Zhou X. Two-stage aging trajectory prediction of LFP lithium-ion battery based on transfer learning with the cycle life prediction. Green Energy Intell Transp 2022;100008.
[9] Zhang Y, Xiong R, He H, Pecht MG. Long short-term memory recurrent neural network for remaining useful life prediction of lithium-ion batteries. IEEE Trans Veh Technol 2018;67(7):5695–705.
[10] Guo W, He M. An optimal relevance vector machine with a modified degradation model for remaining useful lifetime prediction of lithium-ion batteries. Appl Soft Comput 2022;124:108967.
[11] Ma G, Wang Z, Liu W, Fang J, Zhang Y, Ding H, Yuan Y. A two-stage integrated method for early prediction of remaining useful life of lithium-ion batteries. Knowl-Based Syst 2023;259:110012.
[12] Wang J, Deng Z, Li J, Peng K, Xu L, Guan G, Abudula A. State of health trajectory prediction based on multi-output Gaussian process regression for lithium-ion battery. Batteries 2022;8(10):134.
[13] Ma G, Xu S, Jiang B, Cheng C, Yang X, Shen Y, Yang T, Huang Y, Ding H, Yuan Y. Real-time personalized health status prediction of lithium-ion batteries using deep transfer learning. Energy Environ Sci 2022;15(10):4083–94.
[14] Zhao S, Zhang C, Wang Y. Lithium-ion battery capacity and remaining useful life prediction using board learning system and long short-term memory neural network. J Energy Storage 2022;52:104901.
[15] Lyu Z, Wang G, Gao R. Li-ion battery prognostic and health management through an indirect hybrid model. J Energy Storage 2021;42:102990.
[16] Ren L, Dong J, Wang X, Meng Z, Zhao L, Deen MJ. A data-driven auto-CNN-LSTM prediction model for lithium-ion battery remaining useful life. IEEE Trans Ind Inf 2020;17(5):3478–87.
[17] Wang Z, Liu N, Chen C, Guo Y. Adaptive self-attention LSTM for RUL prediction of lithium-ion batteries. Inform Sci 2023;635:398–413.
[18] Cai Y, Li W, Zahid T, Zheng C, Zhang Q, Xu K. Early prediction of remaining useful life for lithium-ion batteries based on CEEMDAN-transformer-DNN hybrid model. Heliyon 2023;9(7).
[19] Han Y, Li C, Zheng L, Lei G, Li L. Remaining useful life prediction of lithium-ion batteries by using a denoising transformer-based neural network. Energies 2023;16(17):6328.
[20] Catelani M, Ciani L, Fantacci R, Patrizi G, Picano B. Remaining useful life estimation for prognostics of lithium-ion batteries based on recurrent neural network. IEEE Trans Instrum Meas 2021;70:1–11.
[21] Xu L, Deng Z, Xie Y, Lin X, Hu X. A novel hybrid physics-based and data-driven approach for degradation trajectory prediction in Li-ion batteries. IEEE Trans Transp Electr 2022.
[22] Wang B, Lei Y, Li N, Li N. A hybrid prognostics approach for estimating remaining useful life of rolling element bearings. IEEE Trans Reliab 2018;69(1):401–12.
[23] Lu J, Xiong R, Tian J, Wang C, Hsu C-W, Tsou N-T, Sun F, Li J. Battery degradation prediction against uncertain future conditions with recurrent neural network enabled deep learning. Energy Storage Mater 2022.
[24] Jones PK, Stimming U, Lee AA. Impedance-based forecasting of lithium-ion battery performance amid uneven usage. Nat Commun 2022;13(1):1–9.
[25] Zhang S-J, Kang R, Lin Y-H. Remaining useful life prediction for degradation with recovery phenomenon based on uncertain process. Reliab Eng Syst Saf 2021;208:107440.
[26] Ma Q, Zheng Y, Yang W, Zhang Y, Zhang H. Remaining useful life prediction of lithium battery based on capacity regeneration point detection. Energy 2021;234:121233.
[27] Zhang J, Jiang Y, Li X, Luo H, Yin S, Kaynak O. Remaining useful life prediction of lithium-ion battery with adaptive noise estimation and capacity regeneration detection. IEEE/ASME Trans Mechatronics 2022.

[28] Russell MB, King EM, Parrish CA, Wang P. Stochastic modeling for tracking and prediction of gradual and transient battery performance degradation. J Manuf Syst 2021;59:663–74.
[29] Eddahech A, Briat O, Vinassa J-M. Lithium-ion battery performance improvement based on capacity recovery exploitation. Electrochim Acta 2013;114:750–7.
[30] Qin T, Zeng S, Guo J, Skaf Z. A rest time-based prognostic framework for state of health estimation of lithium-ion batteries with regeneration phenomena. Energies 2016;9(11):896.
[31] Cui Y, Chen Y. Prognostics of lithium-ion batteries based on capacity regeneration analysis and long short-term memory network. IEEE Trans Instrum Meas 2022;71:1–13.
[32] Zhang Y, Wang C-Y, Tang X. Cycling degradation of an automotive LiFePO4 lithium-ion battery. J. Power Sources 2011;196(3):1513–20.
[33] Ungurean L, Cârstoiu G, Micea MV, Groza V. Battery state of health estimation: a structured review of models, methods and commercial devices. Int J Energy Res 2017;41(2):151–81.
[34] He W, Williard N, Osterman M, Pecht M. Prognostics of lithium-ion batteries based on Dempster–Shafer theory and the Bayesian Monte Carlo method. J Power Sources 2011;196(23):10314–21.
[35] Xing Y, Ma EW, Tsui K-L, Pecht M. An ensemble model for predicting the remaining useful performance of lithium-ion batteries. Microelectron Reliab 2013;53(6):811–20.
[36] Richardson RR, Osborne MA, Howey DA. Gaussian process regression for forecasting battery state of health. J Power Sources 2017;357:209–19.
[37] Li D, Yang L. Remaining useful life prediction of lithium battery using convolutional neural network with optimized parameters. In: 2020 5th Asia conference on power and electrical engineering. ACPEE, IEEE; 2020, p. 840–4.
[38] Yu F, Koltun V. Multi-scale context aggregation by dilated convolutions. 2015, arXiv preprint arXiv:1511.07122.
[39] Zhou D, Li Z, Zhu J, Zhang H, Hou L. State of health monitoring and remaining useful life prediction of lithium-ion batteries based on temporal convolutional network. IEEE Access 2020;8:53307–20.
[40] Lin M, Chen Q, Yan S. Network in network. 2013, arXiv preprint arXiv:1312.4400.
[41] Hochreiter S, Schmidhuber J. Long short-term memory. Neural Comput 1997;9(8):1735–80.
[42] Goodfellow I, Bengio Y, Courville A. Deep learning. MIT Press; 2016.
[43] Tan Y, Zhao G. Transfer learning with long short-term memory network for state-of-health prediction of lithium-ion batteries. IEEE Trans Ind Electron 2019;67(10):8723–31.
[44] Cheng H, Tan P-N, Gao J, Scripps J. Multistep-ahead time series prediction. In: Pacific-Asia conference on knowledge discovery and data mining. Springer; 2006, p. 765–74.